Preliminary Performance Results of a 5-cm Kaufman-Type Ion Thruster

IEPC-2011-135

Presented at the 32nd International Electric Propulsion Conference,
Wiesbaden • Germany
September 11 – 15, 2011

Gilberto M. Sandonato[1], José Américo N. Gonçalves[2] and Ricardo T. Irita[3]

National Institute for Space Research-INPE, São José dos Campos, SP, 12227-010, Brazil

and

Paolo Gessini[4]
University of Brasilia at Gama - UnB Gama, Gama, DF, 72405-610, Brazil

Abstract: **A 5-cm Kaufman-type ion thruster, intended for satellite attitude control, has been under development in the Associated Plasma Laboratory (LAP) at the National Institute for Space Research (INPE) – Brazil. This ion thruster was numerically studied in terms of plasma generation and ion optics system. In addition the experimental setup incorporates new technologies such as hollow cathodes and magnetic containment by a Helmholtz pair, which have never been used in the previous Brazilian prototypes. The preliminary experimental results have shown that thrust levels of about 20 mN can be obtained at specific impulses of 5851 s and at thrust-to-power ratios of 20 μN/W, using argon as propellant.**

Nomenclature

Br	=	remanence
g	=	acceleration of gravity
I_n	=	ion beam current (n=b), ion current per hole (n=h)
I_s	=	specific impulse
L_b	=	ion beam propagation distance (in free space)
$\dot{m}_k$	=	cathode mass flow rate (k=C), main discharge (k=D)
m_i	=	ion mass
N	=	number of grid holes
P	=	perveance
q	=	ion charge
R	=	net-to-total beam voltage ratio
T	=	thrust
V_j	=	accel grid (j=A), discharge (j=D), screen grid (j=S) and beam total voltage (j=T)
α	=	beam divergence angle

---

[1] Senior Researcher, Associated Plasma Laboratory, gms@plasma.inpe.br.
[2] Senior Researcher, Associated Plasma Laboratory, americo@plasma.inpe.br.
[3] Senior Researcher, Associated Plasma Laboratory, irita@plasma.inpe.br.
[4] Associated Professor, Energy Engineering, paologessini@unb.br

I. Introduction

THE development of Kaufman-type ion thrusters began in Brazil in 1985 by the Associated Plasma Laboratory (LAP) at National Institute for Space Research – INPE. The ion thrusters should have low power consumption and a small size to meet the requirements of the satellites of Brazilian Complete Space Mission. Since then, a series of three prototypes were tested and served to demonstrate that such technology is viable in the country.[1] These first prototypes were equipped with very simple technology components, such as tungsten filaments or thermionic oxide cathodes for plasma generation and beam neutralization, stainless steel grids and permanent magnets for magnetic containment. Argon was always the propellant used in the performance tests. Thrust levels starting from 500μN could be increased up to 3 mN along the time by improving the design and technology of the components. However, components, such as the cathodes and permanent magnets, exhibited lifetime too short and their technology should be improved.

The present 5-cm thruster model was, then, designed based on the experience of the previous thrusters, and aimed at testing new technologies such as: hollow cathodes, magnetic coils for magnetic containment and molybdenum grids. Numerical codes were used in the design of this new engine, such as KARAT[2] for the study of plasma generation and magnetic containment quality and IGX[3] to study the grid system.

LAP also established facilities for testing of ion thrusters and hollow cathodes. These facilities include vacuum chambers, power supplies, mass spectrometers, data acquisition systems, and diagnostics such as ion probes and a pendulum target thrust balance[4] (PTB).

II. The 5-cm ion thruster – PION5

The thruster PION5 consists of five main sections: cathode enclosure, anode, grids system magnetic assembly, and neutralizer, as shown in Fig. 1. The cathode enclosure comprises a chamber where there is inside a gas manifold for the main discharge feeding, and a hollow cathode with enclosed keeper and a baffle. The anode is electrically insulated by ceramic insulators from both the cathode enclosure and grids system. The magnetic assembly consists of a Helmholtz pair and a ring permanent magnet radially magnetized. A pair of molybdenum grids electrically insulated by ceramic insulator comprises the grids system. The acceleration grid is attached to the system by a tapered ring which also serves to focus the ion beam, since it is angled shape of Pierce. All these components are surrounded by a metallic piece intended for both electrical and magnetic shieldings. The magnetic shielding is done by both front and the back parts made with Mu-Metal. Finally, both a hollow cathode and an enclosed keeper comprise the neutralizer located outside of the shielding of the thruster.

The major challenge in this ion thruster development was to design and build all its components using the existing facilities and workshops at the institute (INPE). To do it so, preliminary numerical studies were carried out to reach the final conception of the ion thruster.
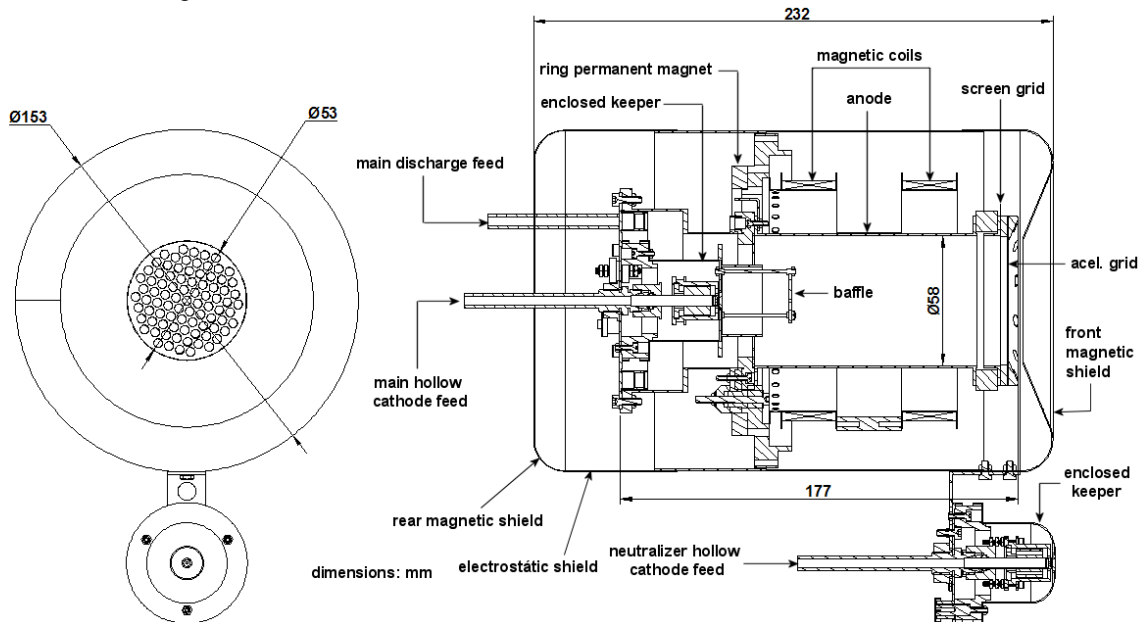

Figure 1. 5-cm Kaufman-type ion thruster schematics (PION5).

A. Plasma generation numerical study

The plasma generation in the discharge chamber (anode region) was studied using KARAT which is a PIC code (particle in cell code) that can solve Maxwell`s equations and the continuity equation as well. Cylindrical symmetry was adopted in the study, with focus on the charge density distribution generated under a given magnetic field distribution.

The magnetic field distribution was numerically obtained for single Helmholtz coils and in the presence of the ring permanent magnet. If only Helmholtz coil was used then the axial magnetic induction is shown by the solid lines curves in Fig. 2 for various coil total current (the term total coil current is used because the coils were electrically connected in parallel). This profile is remarkable changed when a radially magnetized ring permanent magnet ($Br = 4300$ G) is introduced, as shown by the dash lines curves in Fig. 2. The numerical results obtained for the magnetic induction were checked by measuring the magnetic induction using a Gaussimeter probe in a specific location of the Helmholtz coil. Both results were in good agreement, as shown in Fig. 3. The magnetic field lines for the magnetic assembly are shown in Fig. 4.
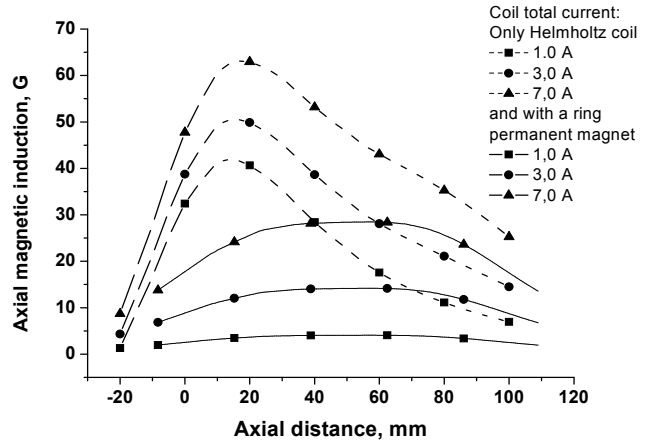
The main input parameters in KARAT were, then, the geometry boundary points, magnetic induction data, ionization and excitation cross sections data for Argon[5], and those ones listed in Table I.

Figure 2. Axial magnetic induction.
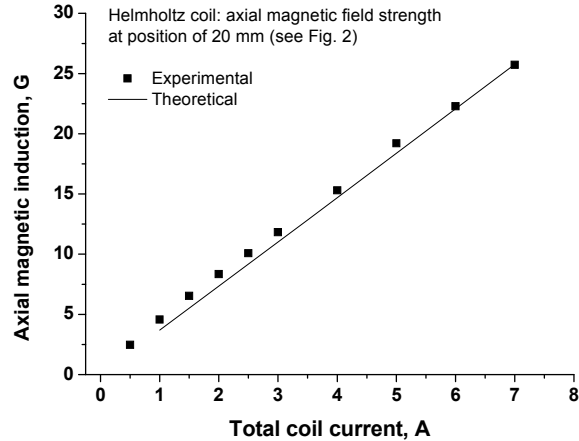

Figure 3. Axial magnetic field induction for the Helmholtz pair.

Table I.   KARAT input parameters.

Input parameter	Value
Propellant atomic mass	40
Neutral atoms density, cm^3	4×10^{12}
Primary electrons current, mA	200
Maximum axial magnetic induction , G	50
Beam voltage (screen), V	1000
Acceleration grid voltage, V	-100
Anode voltage, V	1050
Grids transparency	1
Propellant	Argon

The value of the primary electrons current was intentionally lower than that normally used in the discharge generation practice in order to avoid strong space charge effects during the first run steps of the code. In contrast, a larger neutral atoms density was adopted since the ionization rate is proportional to the product of the primary electron and neutral atoms density.[6] The code adopts the neutral atoms in background and at rest, and once ionized the ions feels the electric field gradients, which change in time as the plasma is generated.
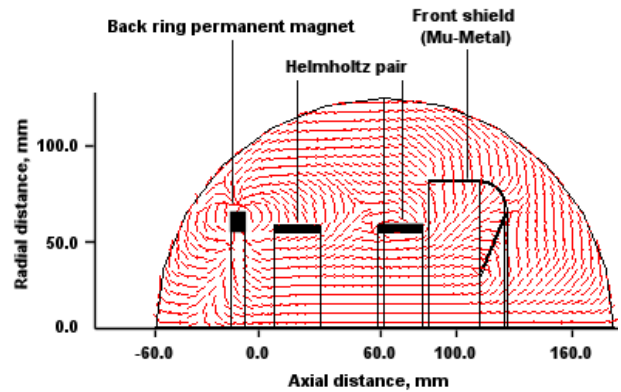
Only the main discharge was studied in the simulations, since the focus was on the capability of plasma generation under the fixed parameters. The simulation ran until a steady state was observed in

Figure 4. Magnetic field lines for half section of the magnetic assembly.

terms of the number of particles generated, as shown in Fig. 5a. Some primary electrons trajectories for an axial magnetic induction of 50 G (see dashed curve for 3.0A coil total current in Fig.2) are shown in Fig. 5b. This value was the best magnetic that allowed plasma volumes within a compatible volume of the discharge chamber. Notice that in the region of the cathode the primary electrons are spinning around the magnetic induction lines with a lower Larmor radius than in the anode region. This is because the magnetic induction decreases downstream the grids facilitating the primary electrons collection by the anode. In practice this suggests a lower discharge voltage. Higher values of the axial magnetic induction the lower will be the plasma volume inside de discharge chamber, thus increasing the discharge voltage and decreasing the beam extraction area at the screen grid as well.

At the steady state the potential profile exhibits values close the anode voltage in the cathode region whereas it is of about 50 V above the anode potential in the main discharge region, as shown in Fig. 5c.

As in the simulations the ion beam in unneutralized the space potential becomes 100V positive to the ground zero potential. The ion density is rather uniform in the main discharge region, as shown in Fig. 5d. The charge peaks in the region of cathode come from the ions that are attracted to the cathode voltage.

The numerical study have also revealed that ion currents of about 10 mA can be extracted from the discharge chamber for a plasma density of 10^{10} cm^{-3}. This ion current will be less if KARAT would take into account the grids transparency, and, thus it will not produce thrusts in mili-Newton range unless the beam voltage is increased substantially. Denser plasmas could increase the ion current proportionally to order of magnitude, but the number of particles was deliberately limited in order to save computational time.

B. Ion optics numerical study

IGX code was used to study the ion optics properties of ion grids system for PION5 thruster. It is a high-speed particle simulation code developed to study ion optics under conditions where the three-dimensional shape of the sheath from which ions are drawn is important. It was developed after experimental observations suggested three-dimensional effects were important under the high voltage operating conditions required in high specific impulse ion thrusters. Screen and accel hole axes are required to be co-linear in the analysis.

This study aimed to establish both geometrical and electrical parameters, such that the ion thruster could produce ion currents in a wide range of values, i.e., that the grids system could be flexible enough to allow severe experimental tests with the ion thruster while keeping the geometrical parameters constants.

(a)

(b)

(c)

(d)
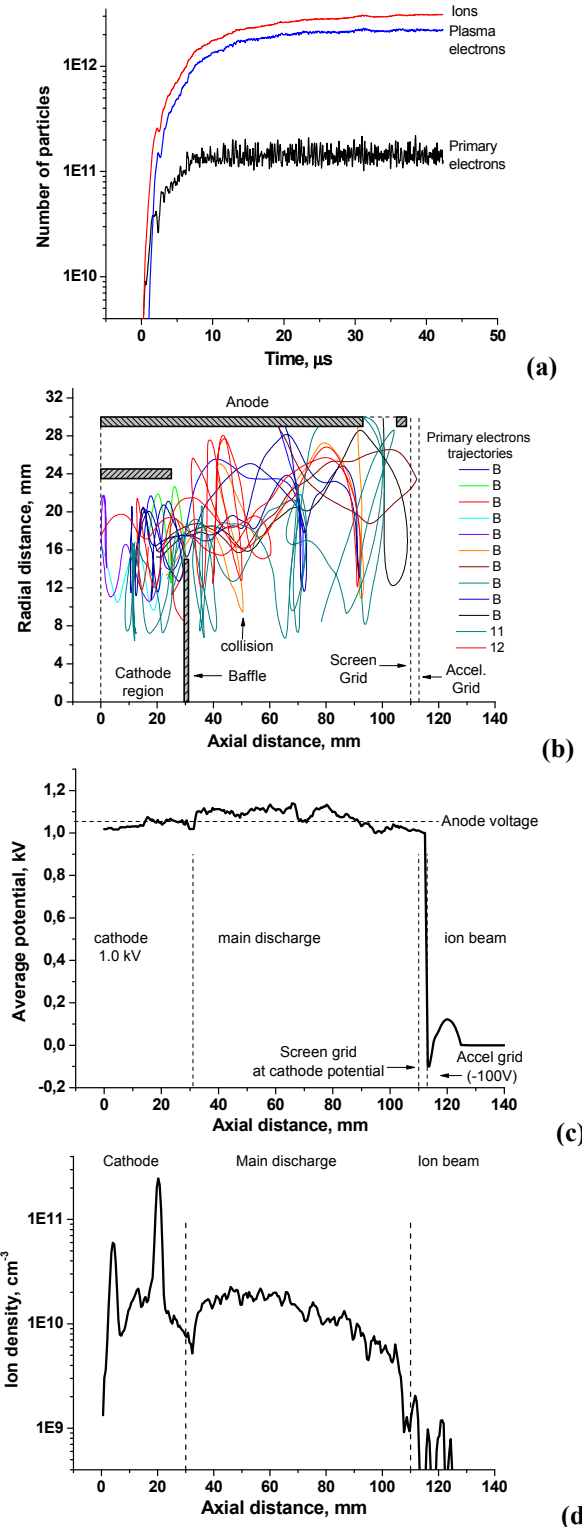
Figure 5. Plasma generation numerical results: number of particles as function of time (a), primary electrons trajectories (b), average potential (c), and ion density (d). Propellant: argon.

The 32nd International Electric Propulsion Conference, Wiesbaden, Germany
September 11 – 15, 2011

Since the thrust for single charged ion beam is given by[6]:

$$T = I_b \sqrt{\frac{2m_i V_T}{q}} \cos\alpha \qquad (1)$$

where

$$V_T = V_S + |V_A| \qquad (2)$$

the ion current per hole is, thus given by:

$$I_h = \frac{T}{N \cos\alpha} \sqrt{\frac{q}{2m_i V_T}} \qquad (3)$$

The net-to-total voltage ratio is expressed by[6]:

$$R = \frac{V_S}{V_T} \qquad (4)$$

Another important parameter that describes the space charge effects in an ion beam is the perveance per hole which is given by:

$$P = \frac{I_h}{V_T^{3/2}} \qquad (5)$$

Using Eqs. 1 to 5 the input parameters for IGX code are, thus, listed in Table II.

Table II. IGX input parameters.

Input parameter		Value
Propellant		Argon
Propellant flow rate, mAeq		0.70
Propellant temperature, K		500
Initial ion kinetic energy, eV		5
Number of holes		1285
Grid beam extraction section, mm		50
Grid hole diameter, mm		1
Hole to hole spacing, mm		1.3
Grid spacing, mm		0.5
Screen grid thickness, mm		0.1
Accel grid thickness, mm		0.5
Grid physical transparency		0.5
Discharge voltage, V		30
R		0.96
P, A/V$^{3/2}$		6.2 x 10^{-6}
T, mN	V_T	I_h (for $\alpha=0^o$)
1	530	37 μA
10	1330	233 μA
20	1891	392 μA

The grid thicknesses adopted in Table I were the ones that correspond to materials available to build them in the laboratory.

The numerical study reveals that the ion beam profile is slightly changed as the thrust level is increased while keeping constant both R and the geometric parameters for the grid system, as shown in the Figs 6a, 6b and 6c (where the upper red circle represents the plasma sheath facing the screen grid). Notice that the ion beam exhibits low divergence for all study cases and therefore α can be really adopted as zero degree in Eq. 1.


(a)

(b)

(c)
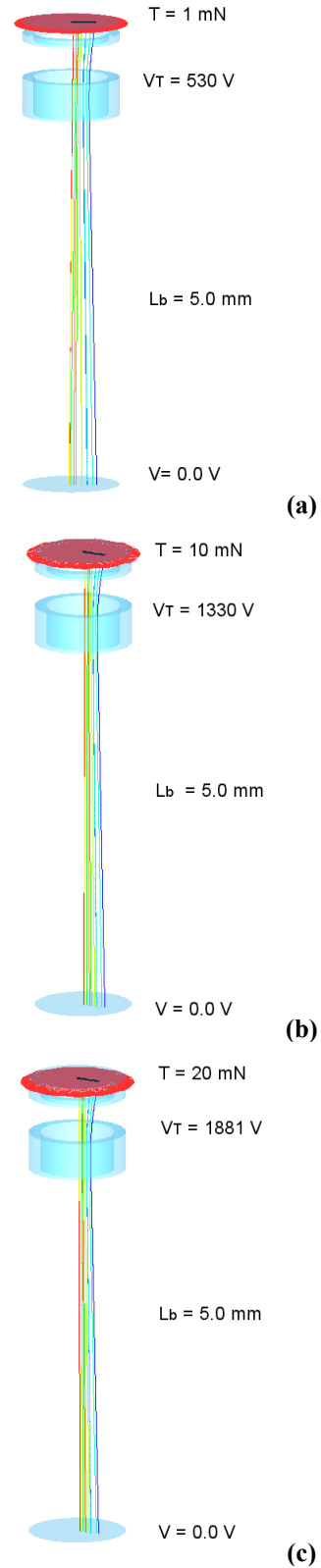
Figure 6. Pion5 ion optics for different thrust levels while keeping constant the geometric grid parameters.

Accel grid voltage is set negative such that it prevents the electrons emitted by the neutralizer from entering the high field region and backstreaming at high energy into the discharge chamber, and to reduce accel grid erosion by the bombardment of backflowing ions as well.

C. Experimental Apparatus and Results

The performance tests with PION5 were carried out in a 1.2 m diameter by 3 m length vacuum chamber pumped by three cryo-cooled diffusion pumps which all performs 6000 l/s of pumping speed for nitrogen. The base pressure of the vessel is 7×10^{-7} mbar and the ultimate pressure is in the range of 1×10^{-5} to 6×10^{-5} depending upon the gas load. Argon was the propellant in all performance tests since it was the gas available at this time. A retarding field energy analyzer (RFEA) and a pendulum target thrust balance are the main diagnostics for ion beam characterization. PION5 is installed on the movable door of the vacuum chamber as shown in Fig. 7.
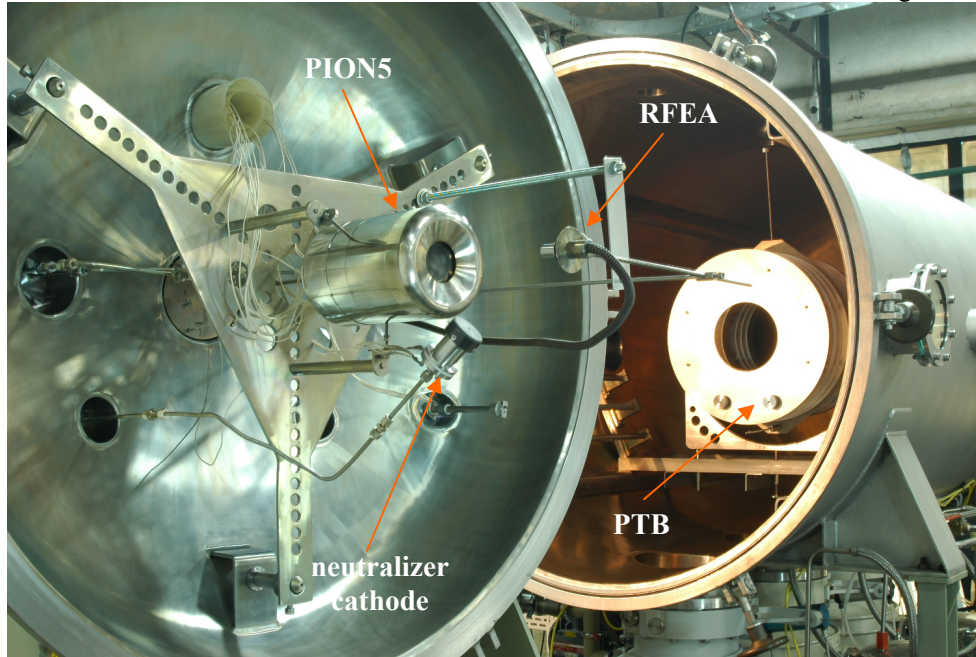
**Figure 7. PION 5 experimental apparatus.**

Mass flow rate measurements and control were made using flowmeters and manual needle valves, respectively. Commercial mass flow controllers were dismissed because they do not maintain the flow set point after the cathodes ignition.

Grade 304 stainless steel was used in the most parts of the thruster body except for the rear and front shields which were made with MU-metal. Alumina and boron nitrate were the main ceramics used to make the insulators.

Screen and accel grid were made with tantalum and their dimensions follow the ones listed in Table II. Their 1285 holes were opened by LASER machining.

The hollow cathode consists of a 5-mm diameter by 40-mm long, 0.3-mm-wall thickness tantalum tube, with a cold-pressed 1-mm diameter orifice tungsten tip. The insert consists of a 5-turns rolled tantalum foil painted with a thin layer of mixed carbonates, $(Ca, Ba, Sr)CO_3$, which are converted to oxides by heating the insert up to 900 °C.

The cathode heater comprises a boron nitride body machined in the shape of a revolver cylinder, in which holes a coiled tungsten filament is passed through. This heater expends 90 W to heat the cathode up the carbonate to oxide conversion temperature. The hollow cathode assembled on the flange containing the main discharge gas manifold is shown in Fig. 8. All cathodes are equipped with enclosed keeper which tip is made of graphite.

The first experimental study aimed to find out how the main discharge was impacted by varying parameters such as magnetic induction and mass flow rate with no ion beam extraction. The magnetic induction was varied by changing the Helmholtz pair total current which relationship is plotted in Fig. 3. Varying the
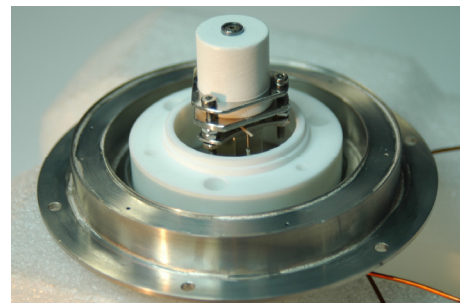
Figure 8. Hollow cathode assembled on the flange of the main discharge gas manifold.

Helmholtz pair total current from 0 a to 6 A the discharge voltage increases from 27.5 V to 47.5 V, for the same 0.21 mAeq in the cathode and main discharge flow rates, as shown in Fig. 9. For the same variation of the total current in the coils, the discharge voltage decreases for a higher mass flow rate of 0.28 mAeq in each of the components mentioned.

The discharge voltage as function of the flow rate in the cathode while keeping constant the flow in the main discharge, and vice versa, is shown in Fig. 10, for 3.0 A of total current in the coils (corresponding to a maximum axial magnetic induction of 50 G in Fig. 3). Notice that discharge voltage exhibits higher values for a variation of the mass flow rate in range of 0.15 mAeq to 0.27 mAeq in the main discharge, while keeping 0.28 mAeq in the cathode. For higher values than 0.3 mAeq for both devices there is no remarkable difference between the gas flow situations. The curve related to the mass flow in the cathode starts at 0.12 mAeq because this is the lower limit in which the main hollow cathode can operate.

The effect of the magnetic field in the thruster is such that it can produce an increase in thrust by increasing the ionic current at screen grid and also to accelerate the ions in the plasma by increasing the discharge voltage. This can be seen in Fig. 11 in which the screen grid current departs from 125 mA reaching 460 mA for a total coil current varying from 3.3 A to 6.5 A. At the same time, the discharge voltage increases from 29 V to 34 V for the discharge current and mass flow rates described in Fig. 11.

Setting the discharge parameters to those ones in Table III, the thruster was, thus, tested in terms of thrust production as function of the total beam voltage. The tests were carried out in two steps. In the first one the total beam voltage was varied and the ion beam current was measured by the RFEA, in order to establish the upper operating limit for the thruster. The RFAE can perform translational and rotational movements. It was positioned at 230 mm apart from accel grid and rotated until a maximum current was measured. Once found the maximum current, the RFEA was, then, rotated again to find the radial distance where the ion current vanished. By doing it so, the beam divergence angle could be estimated (see Appendix). As measurements were made only of current density on the axis of ion beam, was necessary to assume a charge space distribution which with the value of angle of beam divergence the total ion current can be estimated. The space distribution can be assumed as having a rectangular profile (uniform charge density) or a triangular one (see Appendix). This late comes from earlier experimental studies[7] where the beam charge space distribution as function of the beam total voltage suggests that such profile fits the experimental data. The thrust level could be, therefore, estimated using both the total ion beam current and divergence angle in Eq. 1.

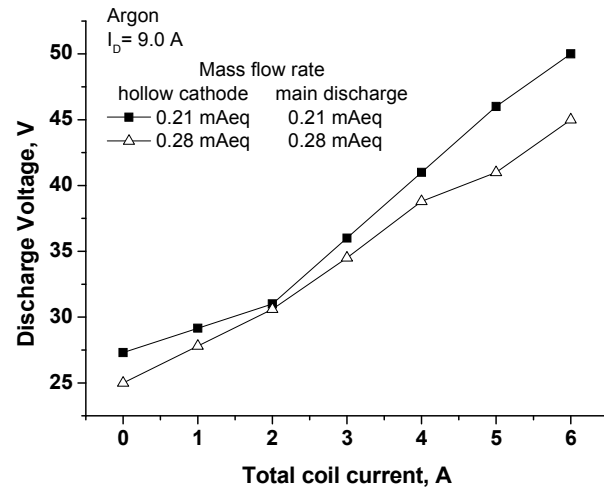In the second step, the RFEA was removed from

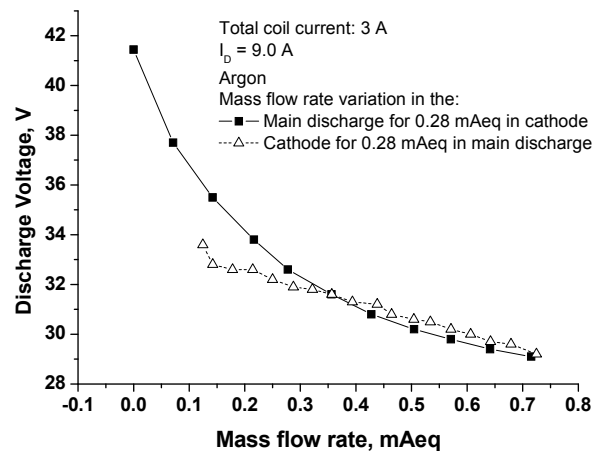Figure 9. Discharge voltage as function of the total current in the coils for different mass flow rate.

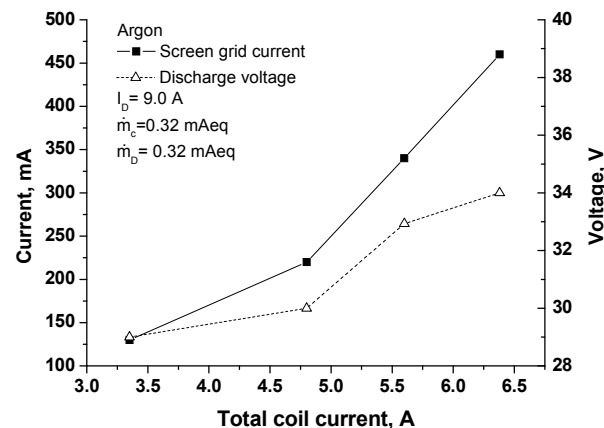Figure 10. Discharge voltage as function of the of mass flow rate.

Figure 11. Discharge voltage as function of total coil current.

7

the ion beam and the total voltage was set at the maximum value (as determined in previous step) and the thrust was measured by the pendulum target balance. Such experimental procedure was adopted to avoid the ion probe from disturbing the thrust measurements by PTB.

The results from RFEA reveal a beam divergence angle of $30°\pm10\%$ which produces thrusts levels (Eq. 1) in the range of 6 mN to 31 mN if a rectangular (uniform) beam density distribution was adopted, and in the range of 3 mN to 19 mN if a beam density triangular distribution, for beam total voltages varying from 350 V to 657 V, as shown in Fig. 12. The maximum beam total voltage was due to sparking inside the vacuum chamber that limited the beam propagation. It is believed that sparking starts because the high ultimate pressure of 5×10^{-5} mbar during the thruster running. Lower ultimate pressures demand improving the vessel pumping speed at least one order of magnitude.

The PTB result was just for only one thrust level because the preliminary tests aimed to find the extreme operating condition of the thruster. This is represented by a single point in Fig. 12 and is equivalent to 21 mN $\pm30\%$. To obtain this value, the PTB was submitted to a series of thrust pulses with duration of 5 min each one. Fig. 13 shows two of these pulses. Notice that a triangular density distribution produces a closer result to the PTB one.

Adopting the triangular charge distribution the total ion beam current estimate is 927 mA for a beam total voltage of 657 V and a screen grid current of 1.2 A. Dividing the total beam current by the screen grid current, the estimate grids transparency is thus 0.77 for the maximum thrust obtained.

Considering the original geometrical parameters of the grids, such thrust level should be impossible to be attainable. Nevertheless, running the engine under the upper value of screen grid current was only possible for few minutes as the electric power dissipated on this grid made it red hot. The thermal stress can produce grid deformation changing the ion optics of the system of grids. The deformation can produce effects such as the misalignment of the holes of screen and accel grids and can approach or space out the grids as well. Assuming that the grids got closer to each other, IGX reveals that 20 mN thrust level can be produced if the grids spacing is reduced to 0.25 mm, as shown in Fig. 14. In this case the beam is more divergent that that one shown in Fig. 6c. This can explain why such high divergence angle was measured during the performance tests.

The specific impulse can be estimate by:

$$I_s = \frac{T}{\dfrac{\dot{m}}{e} m g} \qquad (6)$$

$\dot{m}$ is the total mass flow rate in Aeq. Substituting $\dot{m}$ = 0.81 mAeq (0.34 mg/s), T = 20 mN and g = 10 m/s^2 in Eq. 6, a specific impulse of 5851 s is estimated.

The input power on the thruster sections and the total power involved in thrust production in steady state regime are all listed in Table IV. Using the total input power a thrust-to-total power ratio of 19.8 µN/W is thus estimated.

The main PION5 performance parameters are then compiled in Table V. It is worth to point out that these parameters represents the thruster operation under

Table III. PION5 operating parameters.

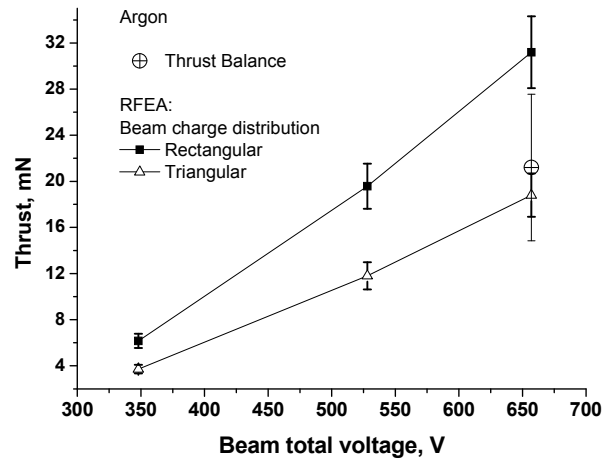| Operating parameter	Value
I_D, A	9
V_D, V	42.5
$\dot{m}_c$, mAeq	0.32
$\dot{m}_d$, mAeq	0.32
Total coil current	6.5
RFEA distance from accel grid, mm	230
PTB distance from accel grid, mm	1400
Neutralizer keeper current, A	1.5
Neutralizer keeper voltage, V	27
Neutralizer mass flow rate, mAeq	0.11

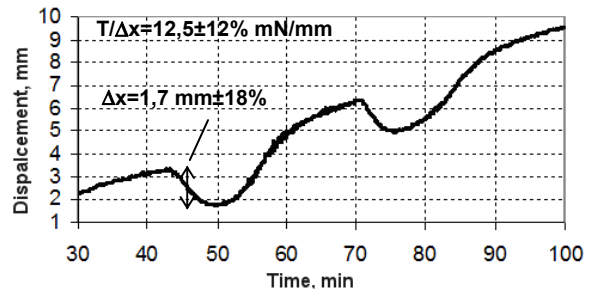**Figure 12. Thrust level as function of beam total voltage. Results from RFEA and PTB.**

Figure 13. PTB displacement under 5 min thrust pulses.

extreme situation.

Table IV. PION5 input power.

Input power, W			
discharge	ion beam	mag. coils	neutralizer
382.5	570.1	15	40.5
Total input power = 1008.1			

Table V. PION5 preliminary performance parameters.

T	I_s	Thrust-to-power ration
20 mN	5851 s	19.8 µN/W

III. Conclusion

The PION5 model has demonstrated an excellent capability on plasma generation thanks to a detailed numerical modeling coupled with the good performance of the cathodes and the field and the flexibility to adjust the magnetic field through magnetic coils to an appropriate magnetic confinement. Nevertheless, the grids system needs further adjustment, mainly concerning the screen grid, in order it can support the heat load while keeping the dimensional stability.

Another matter of attention is the ultimate pressure during the experiments that must be reduced to at least one order of magnitude such that sparking can be minimized if not completely reduced.
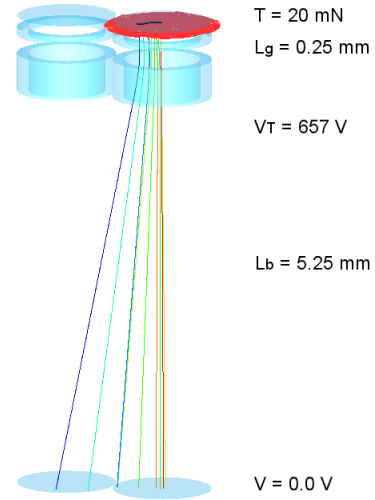
Figure 14. Pion5 modified ion optics.

Appendix

Divergence angle and triangular charge space distribution

The divergence angle is estimated at the ion probe position as

$$\alpha = tg^{-1}\left(\frac{r_b - r_o}{x_c}\right)$$

$$tg(\beta) = \frac{j_o}{r_b - r_c} = \frac{j(r)}{r_b - r}$$

$$j(r) = j_0 \frac{r_b - r}{r_b - r_c} \quad \begin{cases} j(r_c) = j_0 \\ j(r_b) = 0 \end{cases}$$

$$di(r) = j(r) r\, dr\, d\theta \Rightarrow I_b = \frac{j_o}{r_b - r_c}\int_0^{r_b} r(r_b - r)\, dr \int_0^{2\pi} d\theta = \frac{2\pi\, j_o}{6(r_b - r_c)} r_b^3$$

where j_o is the ion probe current density and r_b is the beam radius both at a distance x_c apart the ion thruster, r_o is the radius of the beam exhausting section and I_b is the total ion beam current.
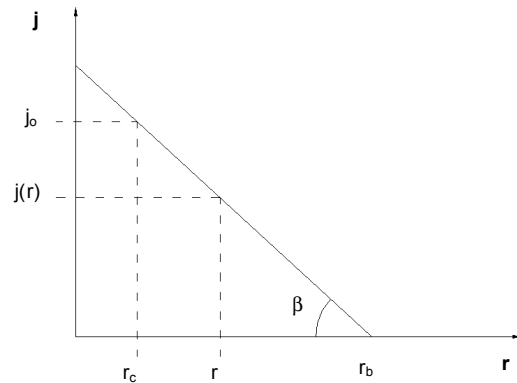
Figure A1. Triangular charge space distribution.

References

[1]Sandonato, G. M., Gonçalves, J. A. N., Irita, R. T., Fernandes, G. F. e, Gessini, P., Marques, R. I. and Gabriel, S. B., "The Brazilian Electric Propulsion Program", IEPC-2007-147, 30th International Electric Propulsion Conference, Florence, Italy, 2007.

[2]KARAT, Software Package, Ver. 9.07, Tarakanov, V., and Simonov, V., karat @ tarak.msk.su, 2007

[3]IGX, Software Package, Ver. 3.0, - 6.12.02, Nakayama, Y., and Farnell, C., Colorado State University, Fort Collins, 2002.

[4]Gessini, P., Sandonato, G. M., Irita, R. T., Gonçalves, J. A. N. and Fernandes, G. F. e, "A Pendulum Target Balance for Ion Engine Thrust Measurement", IEPC-2007-149, 30th International Electric Propulsion Conference, Florence, Italy, 2007.

[5]Rapp., D., and Englander-Golden, P., "Total Cross Sections for Ionization and Attachment in Gases by Electrons Impact. I. Positive Ionization," *The Journal of Chem. Phys.*, Vol. 43, No. 5, 1965, pp. 1464, 1479.

[6]Goebel, D.M., and Katz, I., *Fundamentals of Electric Propulsion: Ion and Hall Thrusters*, JPL Space Science and Technology Series, 2008.

[7]Polk, J. E., Anderson, J. R., Brophy, J. R., Rawlin, V. K., Patterson, M. J., Sovey, J. and Hamley, J., "An Overview of the Results from an 8200 Hour Wear Test of the NSTAR Ion Thruster," AIAA-99-2446, 35th Joint Propulsion Conference & Exhibit, 1999.